Eur. Phys. J. D **11**, 403–411 (2000)

THE EUROPEAN PHYSICAL JOURNAL D

EDP Sciences

The influence of O and C doping on the ionization potentials of Li-clusters

F. Despa[a], W. Bouwen, F. Vanhoutte, P. Lievens, and R.E. Silverans

Laboratorium voor Vaste-Stoffysica en Magnetisme, K. U. Leuven, Celestijnenlaan 200D, 3001 Leuven, Belgium

Received 9 September 1999 and Received in final form 7 February 2000

Abstract. The influence of doping of Li-clusters by electronegative O and C atoms on the ionization potentials was investigated. Experimentally, we report ionization potentials for bare Li_n clusters ($10 \leq n \leq 70$) deduced from photoionization efficiency spectra. The values are compared with the results for Li_nO and Li_nC clusters. Observed differences are largely attributed to a quantum size effect caused by the segregated molecular part around the impurity, which changes the electron work function. Theoretically, the Fermi and exchange-correlation energies which enter the work function, are calculated in the frame of the augmented plane wave (APW) method by taking explicitly into account the presence of the molecular core. The other contribution to the work function, the moment of the double layer at the cluster surface, is computed by solving the corresponding Poisson's equation.

PACS. 36.40.-c Atomic and molecular clusters – 36.40.Cg Electronic and magnetic properties of clusters

1 Introduction

The advent of investigations of binary clusters has drawn the attention upon the stability of atomic micro-objects consisting of metal atoms surrounding an electronegative impurity [1–8]. Some of these show non-stoichiometric structures, *i.e.* the octet rule of the chemical bonding is apparently broken. Such systems are usually called hypervalent molecules [1–7]. However, by increasing the number of metal atoms, the appropriate characteristics of the transition to metallicity appear progressively, accompanying a structural transition. Recent experimental and theoretical studies on metal-rich clusters provided significant information pertaining to segregation between a stoichiometric ionically bound part and the excess metallic component [9–18].

It is the purpose of this paper to examine the effect of the molecular part segregation on the physical properties of such a binary system during the ionization process. We compare the ionization potentials of bare metallic clusters and metallic clusters doped with an electronegative element. The systems under investigation are lithium (Li_n), lithium monoxide (Li_nO) and lithium monocarbide (Li_nC) clusters. The ionization potentials were determined by experiment in the size range $2 \leq n \leq 70$. Observed differences between bare Li_n clusters and C and O doped lithium clusters are attributed to a quantum size effect. The quantum size effect is due to the "molecular" part segregated around the impurity which is confining the valence electrons into a higher density. It perturbs the electronic density of states leading to different internal contributions to the work function. These are explicitly computed in the present work and the effect of the molecular inner core on their values is thoroughly discussed.

In the cluster size range of hypervalent molecules consisting of several metal atoms and an electronegative impurity, the binding seems to have a dominant ionic character. Obviously, the ionization potentials must differ from those of the pure metal systems. Consequently, the ionization potentials of the binary systems will depend on the electronegative character of the solute atom. The fact is quite consistent with traditional chemical concepts.

By increasing the content of metal atoms, the metalization sets in at an early stage. The electronegative dopant localizes an appropriate number of host atoms (according to the stoichiometry rule) forming a "molecular" part inside the host cluster. The molecular part can be described as a barrier in the potential well within which the valence electrons are moving [10]. Therefore, the delocalized electrons are constrained to move in a smaller volume, compared to the bare metal clusters. Assuming that a host metal atom was substituted by an electronegative impurity of radius r_0, the volume of the molecular part can be, crudely, approximated by

$$\frac{4\pi}{3}R^3 = \frac{4\pi}{3}\left[(n-1)\,r_{\rm s}^3 + r_0^3\right] - (n-p-1)\,\frac{4\pi}{3}r_{\rm s,bin}^3, \quad (1)$$

where n is the initial number of free valence electrons in the bare metallic cluster (for simplicity, we shall restrict the discussion to single-valent metals) and p stands for the electrons localized by the electronegative impurity. $r_{\rm s}$ and $r_{\rm s,bin}$ are the inter-electron spaces, being

[a] e-mail: florin.despa@fys.kuleuven.ac.be

proper "metallic" parameters (the Wigner-Seitz radii) for bare and doped metal clusters, respectively. The Wigner-Seitz radius is related to the Fermi wave-vector, k_{F}, by $k_{\mathrm{F}}^3 = 9\pi/4r_{\mathrm{s}}^3$. Indeed, the electron density and Fermi level for doped clusters are no longer the same as for bare metallic ones. A higher confinement of the electrons raises, by the Heisenberg uncertainty principle, their momentum and Fermi energy, $k_{\mathrm{F,bin}} > k_{\mathrm{F}}$. ($k_{\mathrm{F}}$ refers here to the bare metallic cluster.) The internal contributions to the work function are different in the two cases as was already shown by *Burt and Heine* [22]. Moreover, under some circumstances (the statements of the Laue theorem [23]), these parameters may depend on the boundary conditions.

The differences in the values of the ionization potentials for pure metallic clusters and doped ones still persists even for larger cluster sizes, above the domain of hypervalent molecules. These disappear progressively into the metal-rich clusters domain, where the metallic behavior prevails and the perturbation of the "free" electron states due to the "molecular" core is fully screened.

2 Experimental

Threshold photoionization spectroscopy measurements were performed on Li_n, $\mathrm{Li}_n\mathrm{O}$ and $\mathrm{Li}_n\mathrm{C}$ clusters yielding ionization potentials for $2 \leq n \leq 70$. The results for $\mathrm{Li}_n\mathrm{O}$ and $\mathrm{Li}_n\mathrm{C}$ clusters are thoroughly discussed, in references [16,18] and references [17,19], respectively. A brief summary of the cluster source and the experimental procedure is given here. More details can be found in references [16,18].

Clusters are produced by a laser vaporization source employing a moving rectangular target disk. For these studies, the target disk was made out of isotopically enriched ^{7}Li (99.967% enrichment). Material is vaporized at 10 Hz by the second harmonic output of a pulsed Nd:YAG laser. Simultaneously, high purity He gas is released in the source. This creates a supersaturated metal vapor which rapidly condenses and forms clusters. A supersonic expansion into vacuum further cools the clusters and forms a pulsed molecular beam of clusters directed towards the acceleration stage of a reflectron time-of-flight mass spectrometer. The neutral clusters are photoionized by a pulsed laser beam, accelerated by an electrostatic field and mass analyzed in the spectrometer.

Three different laser systems were used for the photoionization of the clusters. An optical parametric oscillator pumped by a Nd:YAG laser and equipped with a frequency-doubling device provides tunable pulsed light in the wavelength range from 225 nm up to 1600 nm, excluding degeneracy gaps around 355 nm and 710 nm. For the work measurements described here the gap at 355 nm was bridged by a frequency doubled pulsed dye laser. The two laser systems enabled us to record mass abundance spectra for ionization photon energies from 3 eV to 5.5 eV, with an energy step of 0.04 eV. The third laser system, an ArF excimer laser, emits laser light at 193 nm (6.4 eV), providing high enough photon energy to ionize all lithium-containing clusters and therefore, is suitable for recording reference mass abundance spectra.

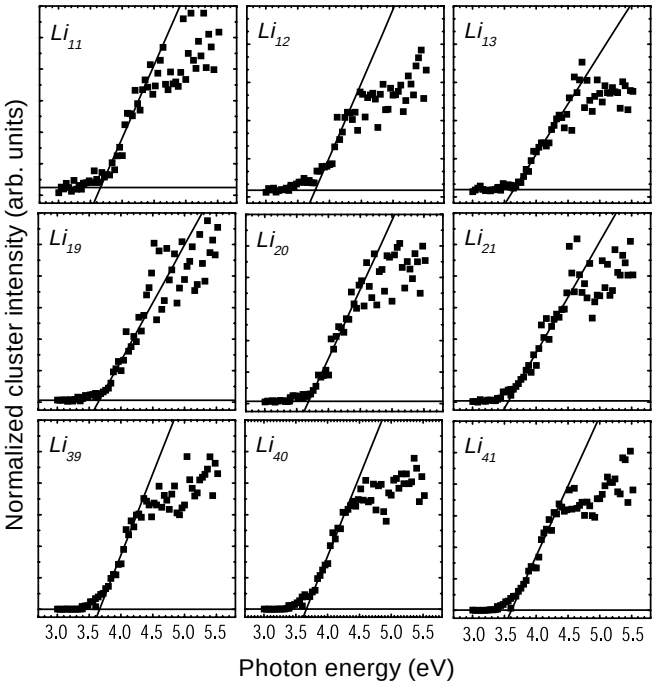

Fig. 1. Photoionization efficiency curves for selected Li_n clusters. The vertical ionization potential is found by extrapolating the first linear rise in the curves towards the baseline (solid line).

Photoionization efficiency (PIE) curves can be constructed by comparing the mass abundances at different ionization photon energies. The influence of production fluctuations in these curves is minimized by proper normalization of the mass abundance spectra using reference mass spectra recorded at 6.4 eV throughout the measurement. Some PIE curves for bare Li_n clusters are shown in Figure 1. Although the bare Li_n clusters have relatively small abundances compared to the more prominent $\mathrm{Li}_n\mathrm{O}$ and $\mathrm{Li}_n\mathrm{C}$ clusters photoionization efficiency curves for Li_n with n ranging from 11 to 70 could be constructed.

From the PIE curves IP values were extracted. They are plotted in Figure 2 together with earlier reported IP's for $\mathrm{Li}_n\mathrm{O}$ [17] and $\mathrm{Li}_n\mathrm{C}$ [16]. For the evaluation of the IP's from the PIE curves, the method of extrapolating the first linear rise in the PIE curves to determine the vertical ionization potential as the point of intersection with the baseline was used [20]. Clearly, this assignment procedure is not unique, but it is generally assumed that linear extrapolation allows to extract the vertical IP of the clusters. In Figure 1, some ionization probability can be noticed below the intercept, which could be attributed to several possible causes. Due to the presence of different chemical bonds with Li clusters in the mass spectrum, it can be expected that there is a contribution of, *e.g.*, CO contaminations in the PIE curves. Unfortunately, the mass resolution of our mass spectrometer is far insufficient to distinguish Li_n and $\mathrm{Li}_{n-4}\mathrm{CO}$ masses (mass difference of only 0.07 atomic mass units). If the pre-threshold signal corresponds to Li_n

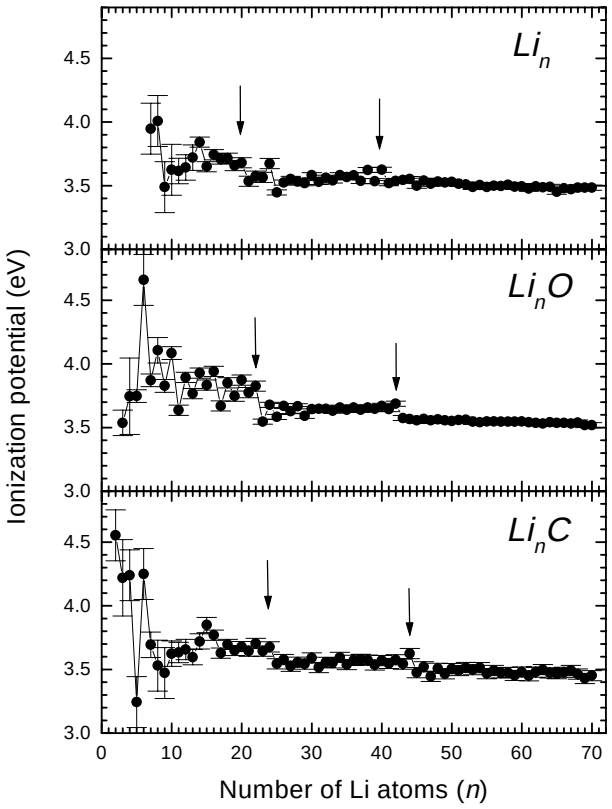

Fig. 2. The experimental ionization potentials of doped and bare lithium clusters as a function of cluster size n: (top) bare lithium clusters, Li_n; (middle) lithium monoxide clusters, Li_nO; (bottom) lithium monocarbide clusters, Li_nC.

ionization, it may indicate an adiabatic IP lower than the parameterized vertical IP. With the low production rate of bare Li clusters and the unknown cluster temperature, we are not able with the present experimental results to be more conclusive on the interpretation of the ionization thresholds. However, the appearance of pronounced steps at 20 and 40 Li atoms in the size dependence of the IP's argues in favor of the present interpretation of the PIE curves.

Ionization potentials for small Li_n clusters ($n \leq 26$) were previously reported by Dugourd *et al.* [21], yielding somewhat lower values for the larger sizes. Although it could be expected that in that experiment the ionization potentials for the larger clusters are somewhat underestimated because of thermal tails in the PIE curves owing to the higher cluster temperature when produced by oven sources, a clearcut comparison with our results cannot be made in view of our adopted IP extraction procedure, as discussed above.

The evolution of the ionization potentials of the doped lithium clusters (see Fig. 2) shows distinct intensity steps at $n = 10,\ 22,\ 42$ for Li_nO and at $n = 24,\ 44$ for Li_nC. This is interpreted as evidence for metallic behavior with $n-2$, respectively $n-4$, delocalized electrons. Deviations from the gradual drop with size of the IP's are clearly absent for small cluster sizes ($n \leq 6$ for Li_nO and $n \leq 16$ for Li_nC). These can be attributed to specific hypervalent bonding mechanisms as is discussed at length in references [16–18]. The ionization potentials of the lithium monoxide cluster are systematically larger (0.1−0.15 eV) than the values of the bare lithium clusters. Although this difference is much smaller for lithium monocarbide clusters, the same trend is observed up to $n = 45$, with a few exceptions.

3 Theoretical

Theoretical calculations within a continuum approach explained qualitatively many properties of metallic clusters [20,24]. Usually, the "Wigner-crystal" model of jellium is employed. Here, the discrete positive ions are replaced by a rigid, uniform, positive background with charge density $+e\overline{n} = 3e/4\pi r_s^3$ (e is the electric charge) inside a sphere of radius R_0. The valence electrons are considered as point charges sitting at equilibrium positions inside the cluster. The only significant potential acting on an electron is that due to the positive background charge within a small volume of radial dimension r_s, that is the Wigner-Seitz cell. The other Wigner-Seitz cells, due to their high symmetry, make only multipole contributions to the potential within the central cell we are considering. These contributions give rise to higher order jellium correction terms.

Generally, the work to eject an electron from a microscopic sized object with metallic characteristics is the ionization energy

$$IP(R_0) = WF + \alpha \frac{e^2}{4\pi\varepsilon_0 R_0} + O(R_0^{-2}). \qquad (2)$$

when R_0 is large compared to the atomic radius. The $R_0 \longrightarrow \infty$ limit yields the work function WF of the planar metallic surface. The second term is the electrostatic energy. ε_0 is the electric permittivity of free space. The quadratic term in $1/R_0$ includes the electronic "spill out" [24]. The actual electron distribution may extend, due to the electron wave nature, outside the cluster surface.

The dimensionless coefficient α entering the electrostatic energy is often used as a fitting parameter for the experimental curves. In a classical approach [25,26], α is given by

$$\alpha\,(r_s) \simeq \frac{1}{2}\left(1 + \frac{z}{9}\frac{r_s^3}{R_0^3} + \frac{z^2}{27}\frac{r_s^6}{R_0^6} + ...\right), \qquad (3)$$

where z stands for the number of electric charges removed from the cluster. For large clusters α equals to 1/2 [20, 24]. For binary clusters r_s in above is replaced by $r_{s,bin}$.

If not specified otherwise, we use throughout this paper the atomic units $a_H = \hbar^2/me^2 = 0.53$ Å (Bohr radius) and $e^2/a_H = 27.2$ eV (twice the Rydberg), which render the square of the electron charge $e^2 = 1$; in addition, we set Planck's constant $\hbar = 1$, so that the electron mass $m = 1$.

To compute the work function for planar metallic surfaces, it is assumed that the lowest electronic states are completely filled, so that the electron is removed from

the highest energy state of the neutral sample, μ. The usual expression for the work function is

$$WF = -\mu, \tag{4}$$

which is reminiscent of Koopmans' theorem for the removal energy of an electron from an atom, with μ the eigenvalue within a self-consistent single-particle approach of the highest occupied state. The WF can then be written as the difference of two parts, (i) the energy required to move the electron through an electrostatic double layer at the surface of the metal sample (ΔV), and (ii) the "binding energy" of the electron ($\varepsilon_{\rm b}$) [27]:

$$WF = \Delta V - \varepsilon_{\rm b}. \tag{5}$$

Here ΔV equals $V_\infty - V_0$, with V_∞ the potential at infinity and V_0 at the planar surface. The "binding energy" is usually calculated without reference to the surface. This is

$$\varepsilon_{\rm b} = \left(\frac{3}{5}\varepsilon_{\rm F} + \varepsilon_{\rm xc}\right), \tag{6}$$

where $\varepsilon_{\rm F}$ is the kinetic (Fermi) energy and $\varepsilon_{\rm xc}$ stands for the exchange ($\varepsilon_{\rm x}$) and correlation ($\varepsilon_{\rm c}$) contributions

$$\varepsilon_{\rm F} = \frac{k_{\rm F}^2}{2};\ k_{\rm F} = \frac{1.92}{r_{\rm s}}; \tag{7}$$
$$\varepsilon_{\rm xc} \cong -\left(\frac{3}{4}\varepsilon_{\rm x} + \varepsilon_{\rm c}\right) = -\frac{3}{4}\frac{0.61}{r_{\rm s}} - \frac{0.44}{r_{\rm s}+7.8}.$$

$\varepsilon_{\rm x}$ and $\varepsilon_{\rm c}$ are usually evaluated at the uniform density of the interior [28,29].

A local density approximation (LDA) as above can give, under certain circumstances, a reasonable value of the $\varepsilon_{\rm xc}$ terms even in a system where the density is far from uniform, LDA results being successfully applied to (large) pure metallic clusters [30]. Also, corrections in the exchange-correlation energy due to the varying electron density at the cluster surface can be included. These are proportional to the density gradient [31,32].

For doped clusters there exists a size range in which the valence-electron density is strongly influenced by the presence of the impurity. In this paper, the molecular inner part formed around the electronegative impurity induces a perturbation of the electronic states, which enhances the Fermi level. This induces a lowering of the electronic interspace ($r_{\rm s}$) by a cluster-size dependent amount. As a consequence, all the quantities expressed in terms of $r_{\rm s}$ are altered. Thus, the intrinsic characteristics of the delocalized electrons, the Fermi level and the exchange and correlation energies, as well as the other parameters ΔV and $\alpha(r_{\rm s})$ entering the ionization potentials (see Eqs. (2, 5)) acquire different cluster size dependent values.

In the following, we define a work function $WF_{\rm bin}$ for binary clusters, which is a function of the inter-electron spacing $r_{\rm s,bin}$, and we evaluate it at every cluster size in the range under investigation. We regard the electrons as free everywhere inside the metallic part of the cluster, and subject to a force only at the boundary with the molecular core. First, the phase shifts of the valence electron waves scattered on the molecular inner core are derived in the frame of the augmented plane wave (APW) method. Then, by summing them with the Friedel sum rule, we extract the Wigner-Seitz radius for each size of the binary cluster.

Due to the finite range and finite depth of the cluster potential, the electrons may "spill out" at the cluster surface. Their density decreases exponentially outside the cluster surface. The outer electrons give rise to a surface potential barrier, ΔV, which contributes to the work function. This contribution is evaluated by solving Poisson's equation with appropriate boundary conditions.

3.1 A simple way to illustrate the change in the work function for doped metallic clusters

3.1.1 Change of Fermi energy

A simple way to show how the molecular inner part of the binary cluster changes the characteristic properties of the remaining delocalized electrons is to restrict consideration to a particular class of potentials. Specifically, it is assumed that around the electronegative impurity one takes an appropriate spherically symmetric potential, delimited by a sphere of radius R (the molecular part). For the binary clusters considered here, R can be written as a function of $r_{\rm s}$ and $r_{\rm s,bin}$ according to equation (1). Outside the inscribed sphere, in the metallic part, one chooses the potential to be constant. Therein, the valence electrons move freely. Potentials of this type are frequently called "muffin-tin" potentials. Of course, actual cluster potentials will not be of this form, and it must be assumed (or hoped) that not too much violence is done to whatever real problem is being studied by this approximation.

With the above approximation to the potential, the electronic wave function can be expanded in a set of functions composed of plane waves in the outer region of the inscribed sphere (the metallic part of the cluster), and a sum of spherical waves in the interior (the molecular part). This is the augmented plane wave (APW) method [34]. A single augmented plane wave is defined to be the function

$$\Phi_{\mathbf{k}} = a_0 \vartheta(r-R)\exp(\mathrm{i}\mathbf{k}\cdot\mathbf{r}) + \sum_{l,m} a_{lm}\vartheta(R-r)R_l(\varepsilon_{\mathbf{k}},r)Y_{lm}(\theta,\varphi). \tag{8}$$

The function $\vartheta(r-R)$ is a unit step function and $R_l(\varepsilon_{\mathbf{k}},r)$ is a solution of a radial wave equation normalized to unity inside the inscribed sphere of radius R. $\varepsilon_{\mathbf{k}}$ is the energy of the electron having the wave vector $\mathbf{k}$. The coefficients a_{lm} are chosen so that the function $\Phi_{\mathbf{k}}$ is continuous across the sphere,

$$a_{lm} = 4\pi i^l a_0 Y_{lm}^*(\theta_{\mathbf{k}},\varphi_{\mathbf{k}})\frac{j_l(kR)}{R_l(\varepsilon_{\mathbf{k}},R)}. \tag{9}$$

$Y_{lm}(\theta_{\mathbf{k}},\varphi_{\mathbf{k}})$ are *spherical harmonics*, j_l stand for *spherical Bessel functions* and $\theta_{\mathbf{k}}$ and $\varphi_{\mathbf{k}}$ refer to the direction

of the electron wave vector $\mathbf{k}$. The constant a_0 has to be determined from the normalization condition.

Equation (9) implies that $\Phi_{\mathbf{k}}$ would be continuous at R. Actually, a plane wave cannot in general be joined smoothly onto spherical waves in the interior of some region, there must be scattered waves as well. The scattering phase shifts can be obtained through the relation [34]

$$\tan\delta_l = \frac{\frac{1}{kR_l}\frac{\mathrm{d}R_l}{\mathrm{d}r}n_l(kR) - n_l'(kR)}{\frac{1}{kR_l}\frac{\mathrm{d}R_l}{\mathrm{d}r}j_l(kR) - j_l'(kR)}, \tag{10}$$

which involves the logarithmic derivative of the radial wave function R_l, $(1/R_l)(\mathrm{d}R_l/\mathrm{d}r)$, evaluated on the inscribed sphere. n_l are *spherical Neumann functions* and the prime indicates derivative with respect to the argument of the function.

Equation (10) yields the phase shifts δ_l owing to the scattering plane wave (a free electron in the metallic region of the cluster) on the perturbation potential produced by the molecular segregated part around the electronegative impurity. Evidently, the perturbation changes the number of states per unit increment of k. The amount of the density of states fetched by the perturbation effect is $(1/\pi)(\mathrm{d}\delta_l/\mathrm{d}k)$. The total change in the number of states up to some particular value of k, considering all l values and the $(2l+1)$ substrates for each l, is given by the Friedel sum rule [34]

$$\frac{1}{\pi}\sum(2l+1)\,\delta_l(\varepsilon_{\mathrm{F}}) = \frac{Z_{\mathrm{e}}}{2}\cdot \tag{11}$$

Here, it is assumed that the impurity has an effective nuclear charge Z_{e} units greater than that of the host. According to (11), the condition of screening of the perturbation at large distances is fully satisfied by bringing $Z_{\mathrm{e}}/2$ states below the Fermi level.

In this way, by using equations (1, 10, 11) we can determine the change of the Fermi level ε_{F} and inter-electron spacing $r_{\mathrm{s,bin}}$, induced by the action of the inner molecular part on the remaining free (valence) electrons. The change of the Fermi level (and electron density) of the clusters under consideration is related to both the remaining volume of valence electrons and the extra nuclear charge brought by the electronegative impurity. It also depends on the appropriate wave function which describes the behavior of the localized electrons in the molecular part.

The present approach disregards additional effects due to the non-uniform electron density at the interface between the molecular and metallic part. Therefore, the calculated Fermi energies could be somewhat underestimated in this work.

Looking at equation (1) we may observe that by making $p = 0$ and $r_0 \equiv r_{\mathrm{s,bin}} = r_{\mathrm{s}}$, R equals the inter-electron spacing r_{s}. This corresponds to the case of pure metallic clusters. Thus, within the APW method, the behavior of the electrons in a pure metallic clusters is described by plane waves with a certain spherically symmetric perturbation at the origin.

3.1.2 The moment of the electric double layer on the cluster surface

The moment of the electric double layer on the cluster surface is defined as the difference in potential between a point outside the surface (V_∞) and a point on the surface (V_0). The position of the reference point is somewhat arbitrary (it can also be in the interior), but once chosen, it fixes the prefactors in the kinetic and exchange-correlation energies for the electrons [27]. The double layer is due to the fact that the actual electron distribution may extend outside the limit of the surface ions (outside the R_0 limit, in our case) and may presumably have sizable density. Therefore, we focus in the following on the calculus of the electron density outside the cluster surface. Once the density of the outer electrons is determined, we calculate the change in electrostatic potential across the dipole layer created by the "spilling out" of electrons at the surface.

Generally, the electron density can be written as

$$\rho(r) = \sum_{\mathbf{k}} |\Phi_{\mathbf{k}}(\mathbf{r})|^2\,\vartheta(\mu - \varepsilon_{\mathbf{k}}), \tag{12}$$

where $\Phi_{\mathbf{k}}(\mathbf{r})$ is the appropriate electron wave function. An electron outside the cluster surface may be described in our case by a wave function decreasing exponentially from the cluster surface, that is the asymptotic form of the *Henkel functions* of the first kind,

$$u_{\mathbf{k}}(\mathbf{r}) = \sum_{l,m} \mathrm{e}^{-kr} b_{lm} Y_{lm}(\theta,\varphi), \quad r > R_0. \tag{13}$$

The electron wave function (13) has to satisfy also the continuity requirement at the cluster surface. Therefore, the coefficients b_{lm} are fully determined by joining the outer electron wave function (13) with that corresponding to the inner electrons (8) at $r = R_0$,

$$b_{lm} = 4\pi a_0 i^l \mathrm{e}^{kR_0} j_l(kR_0)\, Y_{lm}^*(\theta_{\mathbf{k}},\varphi_{\mathbf{k}}), \tag{14}$$

and imposing the required normalization condition

$$|a_0|^2\,\omega + \sum_{l,m}|a_{lm}|^2 + \sum_{l',m'}|b_{l'm'}|^2 = 1, \tag{15}$$

where ω is the volume of the metallic part.

The rule for converting summations over quantum numbers in (12) into integration over wave number $\mathbf{k}$, gives simply

$$\rho_{\mathrm{out}}(\mathbf{r}) = \frac{\Gamma}{(2\pi)^3}\int_0^{k_{\mathrm{F}}} \mathrm{d}k\ \left(k_{\mathrm{F}}^2 - k^2\right)\int \mathrm{d}\Omega_{\mathbf{k}}\,|u_{\mathbf{k}}(\mathbf{r})|^2, \tag{16}$$

for the density of the outer electrons. The volume Γ in above is established by embedding the cluster under investigation in a supersphere of a variable volume $\left(\Gamma = (4\pi/3)\,R_{\mathrm{out}}^3\right)$ containing presumably all the outer electrons.

The change in electrostatic potential across the dipole layer created by the "spilling out" of electrons at the

surface, ΔV, is then given by the solution of Poisson's equation

$$\Delta V = 4\pi\rho\left(\mathbf{r}\right), \qquad r > R_0. \tag{17}$$

Equation (17) may be solved for V by imposing the following boundary conditions (if the cluster is uncharged):

$$\begin{aligned} &V = 0\,,\ \frac{\mathrm{d}V}{\mathrm{d}r} = 0\,,\ \text{as } r \to \infty, \\ &\frac{\mathrm{d}V}{\mathrm{d}r} = 0\,, \qquad\qquad \text{as } r \to R_0. \end{aligned} \tag{18}$$

We can observe that in a "free electron" approximation the last condition in the above requires that

$$\lim_{r \to R_0} \int_r^\infty \rho\left(r\right) \mathrm{d}r = 0.$$

Its physical meaning is that ΔV will be zero if the electron distribution is constant for $R < r < R_0$ and zero for $r > R_0$. We shall make the approximation that, for our "free electron" model, the potential at the cluster surface V_0 will be, by definition, the moment of the surface double layer

$$\Delta V \equiv V_0. \tag{19}$$

Within the present theoretical model, the barrier at the cluster surface is essentially due to Coulomb forces and depends on the cluster size and Fermi energy. Note that, by the continuity requirement of the wave function at the cluster surface, the outer electrons preserve the information about the perturbation introduced by the molecular core.

At this point, one additional comment should be made with respect to the present theory. It was shown that the exchange and correlation forces have a major role in determining the moment of the dipole barrier at the surface, while the Coulomb forces become less important [27, 35–37]. We must note that, actually, the ordinary electrostatic potential contributes slightly to the moment of the dipole barrier only in the large limit of valence electron number of macroscopic samples where the screening among the electrons is high and the potential has a smooth oscillating behavior, therefore. This is, for example, the case of the jellium model. According to the Budd-Vannimenus theorem, the potential at the jellium surface is lowered, in the limit of dominance of bulk properties, by a constant amount determined by the combined exchange and correlation terms [33]. For microscopic sized objects, the screening inside the cluster will be lowered and the balance among various contributions to the effective cluster potential will be somewhat changed. Also, the curvature of the surface can play an important role. The electric field, which contains the outer electrons, will act more profoundly to expel the positive charge near the surface, in this case. The potential barrier at the cluster surface must depend on the cluster size.

4 Results

We determine the change of the Wigner-Seitz radius, $r_{\mathrm{s,bin}}$ (and the Fermi energy $\varepsilon_{\mathrm{F,bin}}$), induced by the interaction of the remaining "free" electrons with the "molecular" core. In order to do that, we solve the system of equations given by (10, 11) where the approximate size of the inner molecular part of the cluster is derived from (1). The parameter r_0 (see Eq. (1)) is identified here with the covalent radius of the impurity. Therefore, we used $r_0 = 1.38$ a.u. for O and $r_0 = 1.45$ a.u. for C, respectively [38]. The quantity Z_{e} entering (11), which measures the difference between the effective nuclear charge of the electronegative impurity and that corresponding to the host atom was calculated according to Slater's rules. This is 2.6 for carbon doped lithium clusters and 3.9 for the oxygen doped lithium clusters. For the radial wave function R_l, we used a Gaussian function

$$R_l = r^{\nu+l} \exp\left(-\gamma r^2\right), \tag{20}$$

normalized to unity inside the inscribed sphere of radius R. ν is the principal quantum number of the impurity valence shell and γ a parameter determined by a fitting procedure. Thus, the value of γ was varied to approach in the limit of large cluster sizes ($n \gg 70$) the Wigner-Seitz radius for pure lithium ($r_{\mathrm{s}} = 3.24$ a.u.) [39]. The values of γ we found are 0.168 for $\mathrm{Li}_n\mathrm{O}$ clusters and 0.19 for $\mathrm{Li}_n\mathrm{C}$ clusters, respectively.

The inter-electron spacing $r_{\mathrm{s,bin}}$ against the cluster sizes n are displayed in Tables 1 and 2. For both binary systems, these are smaller in comparison with the corresponding value of bare lithium ones. We can observe that in the domain of small clusters ($n \lesssim 30$), the $r_{\mathrm{s,bin}}$ parameter for the $\mathrm{Li}_n\mathrm{C}$ system seems to be much more affected by the molecular part in comparison with the $\mathrm{Li}_n\mathrm{O}$ system. This is due to the fact that the carbon atom localizes 4 of the host lithium atoms and the molecular part is larger for the $\mathrm{Li}_n\mathrm{C}$ clusters. Therefore, the valence electrons are more strongly confined in the remaining metallic part. For the cluster sizes of our interest, the inter-electron spacing spreads between 3.138 a.u. and 3.197 a.u., for $\mathrm{Li}_n\mathrm{O}$ and between 3.111 a.u. and 3.2 a.u., for $\mathrm{Li}_n\mathrm{C}$. The above arguments show that the size of the molecular inner part plays an important role in the present model.

All the internal contributions to the "binding" energy ε_{b} (see Eq. (6)) entering the work function WF_{bin} are simply computed by using equation (7) with the corresponding Wigner-Seitz radii derived as above.

The potential barriers V_0 were computed by solving numerically Poisson's equation (17) under the boundary conditions given by equations (18). The integration mesh in real space was over the radial distance between R_0 and R_{out}, which is presumably the distance of the "spilling out" of electrons at the cluster surface. The electric field due to the outer electrons must vanish over this distance. In our calculus, R_{out} was set to $1.3R_0$. The fraction of the outer electrons was renormalized for every cluster size. The experimental ionization potentials for the $\mathrm{Li}_n\mathrm{O}$ system were reproduced with a good accuracy in the limit

Table 1. The theoretical values for Wigner-Seitz radii ($r_{s,bin}$) and the surface potential barriers of the Li_nO system for the cluster sizes ($15 \leq n \leq 70$) .

n	$r_{s,bin}$ (a.u.)	V_0 (eV)	n	$r_{s,bin}$ (a.u.)	V_0 (eV)
15	3.138	0.230	43	3.177	0.399
16	3.139	0.250	44	3.178	0.402
17	3.140	0.270	45	3.179	0.405
18	3.142	0.285	46	3.180	0.408
19	3.143	0.300	47	3.180	0.411
20	3.144	0.310	48	3.181	0.414
21	3.145	0.314	49	3.182	0.417
22	3.148	0.318	50	3.183	0.420
23	3.149	0.322	51	3.184	0.422
24	3.150	0.325	52	3.185	0.424
25	3.153	0.330	53	3.186	0.426
26	3.154	0.335	54	3.187	0.428
27	3.156	0.340	55	3.188	0.430
28	3.158	0.345	56	3.189	0.433
29	3.160	0.350	57	3.189	0.436
30	3.160	0.355	58	3.190	0.439
31	3.162	0.357	59	3.190	0.442
32	3.163	0.359	60	3.190	0.445
33	3.164	0.362	61	3.191	0.447
34	3.166	0.366	62	3.192	0.449
35	3.168	0.369	63	3.192	0.452
36	3.169	0.372	64	3.193	0.455
37	3.170	0.375	65	3.194	0.460
38	3.171	0.380	66	3.194	0.463
39	3.172	0.385	67	3.195	0.466
40	3.174	0.390	68	3.195	0.469
41	3.175	0.393	69	3.196	0.472
42	3.176	0.396	70	3.197	0.475

Table 2. The same as above for the Li_nC system for the cluster sizes ($16 \leq n \leq 70$) .

n	$r_{s,bin}$ (a.u.)	V_0 (eV)	n	$r_{s,bin}$ (a.u.)	V_0 (eV)
16	3.111	0.220	44	3.180	0.318
17	3.116	0.224	45	3.181	0.322
18	3.120	0.227	46	3.182	0.326
19	3.125	0.231	47	3.183	0.331
20	3.130	0.235	48	3.184	0.334
21	3.133	0.237	49	3.185	0.338
22	3.136	0.240	50	3.186	0.340
23	3.140	0.243	51	3.187	0.344
24	3.143	0.246	52	3.188	0.348
25	3.145	0.249	53	3.189	0.352
26	3.148	0.252	54	3.190	0.356
27	3.150	0.255	55	3.190	0.360
28	3.153	0.259	56	3.191	0.364
29	3.155	0.262	57	3.192	0.366
30	3.158	0.265	58	3.192	0.370
31	3.160	0.269	59	3.193	0.372
32	3.162	0.273	60	3.194	0.375
33	3.164	0.276	61	3.194	0.377
34	3.166	0.279	62	3.195	0.380
35	3.168	0.282	63	3.196	0.383
36	3.169	0.285	64	3.197	0.385
37	3.170	0.290	65	3.197	0.388
38	3.172	0.293	66	3.198	0.392
39	3.173	0.297	67	3.198	0.397
40	3.174	0.300	68	3.199	0.404
41	3.176	0.304	69	3.199	0.408
42	3.178	0.308	70	3.200	0.412
43	3.179	0.312			

of large clusters (see Fig. 3b) for a fraction of outer electrons equal to $f_{Li_nO} = 0.195$. The fraction of outer electrons we found for Li_nC clusters (f_2) is larger in comparison with Li_nO clusters, a good agreement with the experimental data (see Fig. 3c) being obtained for $f_{Li_nO} = 0.22$. The larger size of the molecular inner core of the Li_nC system seems to produce a stronger "spilling out" effect of the valence electrons. In the case of pure Li_n clusters, the fraction of the outer electrons, which leads to a good fit to the experimental data, is about $f_{Li_n} = 0.175$ from the entire amount of delocalized electrons. We can observe that the amount of outer electrons we found for each system we investigated is in direct proportion to the geometrical dimension of the perturbation center.

In Tables 1 and 2, the values for V_0 of lithium monoxide and lithium monocarbide clusters are displayed for each cluster size n in the investigated size range with the calculated values for the inter-electron space. In Table 3, the same as above is shown for bare lithium clusters except for the Wigner-Seitz radius which was set to the bulk value $r_s = 3.24$ a.u. [39]. The small differences one can observe among the values of the surface potential barriers at the same cluster size of different systems are due to the presence of the perturbation center. The perturbation induced by the "molecular" core is equally felt by all the valence electrons, including the outer ones. Anyway, these differences disappear progressively with increasing cluster size, the perturbation due to the electronegative impurity being fully screened in the limit of large cluster sizes.

Another observation apparent in Tables 1, 2 and 3 is the increasing trend for V_0 towards large cluster sizes. This can be understood by taking into account the amount of outer electrons at each cluster size. The number of the "spilling out" electrons is directly related to the cluster size, which increases with increasing cluster size. Consequently, the outer field, which is a measure of the outer electron number, is very sensitive to the cluster size. Therefore, the values for V_0 increase slightly with increasing cluster size and approach asymptotically the value for a planar surface of a macroscopic sample. A self-consistent calculation of the effective potential yields $V_0 = 0.6061$ eV for $r_s = 3$ a.u. and $V_0 = 0.5967$ eV for $r_s = 4$ a.u. for a planar surface [40]. From the present approach, we estimate that the value of the planar surface potential barrier is reached for a number of about 100 atoms. From this limit on, the surface potential barrier becomes independent of the cluster size.

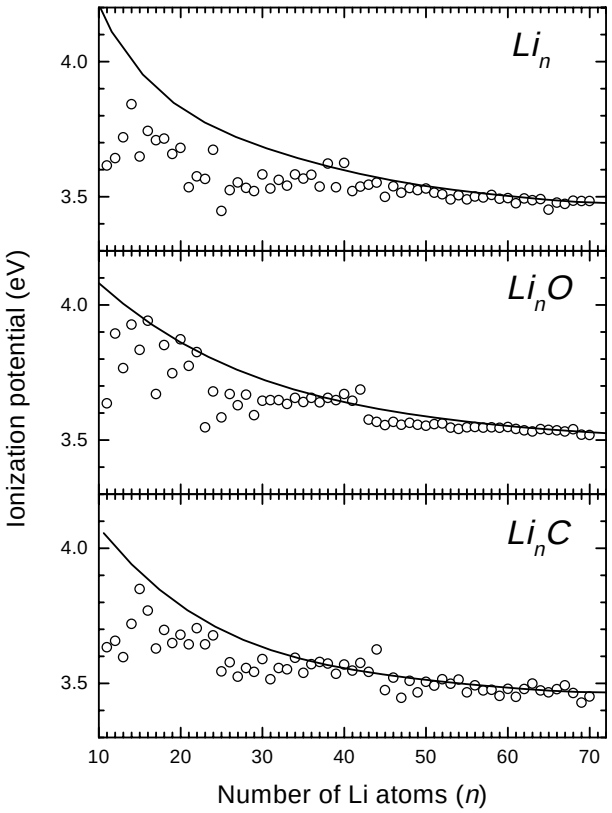

Fig. 3. The theoretical ionization potentials (solid line) compared with the corresponding experimental ones (open dots) as a function of cluster size n: (top) bare lithium clusters, Li_n; (middle) lithium monoxide clusters, Li_nO; (bottom) lithium monocarbide clusters, Li_nC.

Table 3. Theoretical surface potential barriers (V_0) of Li_n clusters ($10 \leq n \leq 70$).

n	V_0 (eV)	n	V_0 (eV)	n	V_0 (eV)
10	0.180	31	0.286	52	0.356
11	0.185	32	0.292	53	0.359
12	0.190	33	0.298	54	0.362
13	0.195	34	0.303	55	0.365
14	0.200	35	0.305	56	0.368
15	0.205	36	0.308	57	0.371
16	0.210	37	0.312	58	0.374
17	0.215	38	0.315	59	0.377
18	0.220	39	0.317	60	0.380
19	0.225	40	0.320	61	0.383
20	0.230	41	0.323	62	0.386
21	0.235	42	0.325	63	0.389
22	0.240	43	0.328	64	0.392
23	0.245	44	0.331	65	0.395
24	0.250	45	0.334	66	0.398
25	0.255	46	0.337	67	0.401
26	0.260	47	0.340	68	0.404
27	0.265	48	0.343	69	0.407
28	0.270	49	0.346	70	0.410
29	0.275	50	0.350		
30	0.280	51	0.353		

5 Conclusions

Ionization potentials of lithium clusters containing up to 70 atoms were compared to the ionization potentials of lithium clusters doped by electronegative impurities (oxygen and carbon).

Observed differences in the values of the size dependent ionization potentials are mainly attributed to a quantum size effect due to the molecular core segregated around the impurity which acts to confine the valence electrons into a higher density. This perturbs the electronic density of states leading to different internal contributions to the work function. The change of the metallic characteristics of the binary cluster is therefore a measure of the perturbation strength induced by the electronegative impurity and is observed in the ionization potentials.

The segregation of the molecular part around the electronegative impurity can also be seen as a local change of the interatomic potential and chemical bond lengths. Then, restoring forces acting against formation of the curved interface between "metallic" and "molecular" parts of the cluster will appear, a fact which can be expressed in terms of interface tension. Furthermore, if one wishes to consider the discrete nature of the binary system, a configurational entropy term due to the different combinations of atoms that constitute the "molecular" and "metallic" parts can be straightforwardly defined.

In conclusion, the metallic characteristics of metal clusters doped with electronegative impurities are significantly altered at small cluster sizes mainly due to the quantum size effect. The metallic characteristics definitely predominate in the range of larger cluster sizes where the perturbation of the "free" electron states due to the "molecular" core is fully screened.

This project is financially supported by the Belgian Fund for Scientific Research – Flanders (F.W.O.), by the Flemish Concerted Action (G.O.A.) Research Program, and the Interuniversity Poles of Attraction Programme (I.U.A.P.) – Belgian State, Prime Minister's Office – Federal Office for Scientific, Technical and Cultural Affairs. F.D. is a Visiting Postdoctoral Fellow and P.L. a Postdoctoral Researcher of the F.W.O. W.B. thanks the Flemish Institute for Scientific-Technological Research (I.W.T.) for financial support.

References

1. C.H. Wu, H. Kudo, H.R. Ihle, J. Chem. Phys. **70**, 1815 (1979).
2. P.v. Ragué Schleyer, E.-U. Würthwein, J.A. Pople, J. Am. Chem. Soc. **104**, 3839 (1982); P.v. Ragué Schleyer, E.-U. Würthwein, E. Kaufmann, T. Clark, J.A. Pople, J. Am. Chem. Soc. **105**, 5930 (1983); P.v. Ragué Schleyer, in *New Horizons of Quantum Chemistry*, edited by P.O. Löwdin, B. Pullman (Reidel, Dordrecht, The Netherlands, 1983), p. 95; P.v. Ragué Schleyer, J. Kapp, Chem. Phys. Lett. **255**, 363 (1996).
3. H. Kudo, Nature **335**, 432 (1992); H. Kudo, K. Yokoyama, Bull. Chem. Soc. Jpn **69**, 1459 (1996).

4. E. Rehm, A.I. Boldyrev, P.v. Ragué Schleyer, Inorg. Chem. **31**, 4834 (1992).
5. C.J. Marsden, Chem. Phys. Lett. **245**, 475 (1995).
6. C. Yeretzian, U. Röthlisberger, E. Schumacher, Chem. Phys. Lett. **237**, 334 (1995).
7. R.O. Jones, A.I. Lichtenstein, J. Hutter, J. Chem. Phys. **106**, 4566 (1997).
8. V. Bonačić-Koutecký, J. Pittner, R. Pou-Amerigo, M. Hartmann, Z. Phys. D **40**, 445 (1997).
9. T. Bergmann, H. Limberger, T.P. Martin, Phys. Rev. Lett. **60**, 1767 (1988).
10. H. Limberger, T.P. Martin, J. Chem. Phys. **90**, 2979 (1989).
11. G. Rajagopal, R.N. Barnett, U. Landman, Phys. Rev. Lett. **67**, 727 (1991).
12. P. Weis, C. Ochsenfeld, R. Ahlrichs, M.M. Kappes, J. Chem. Phys. **92**, 2553 (1992).
13. C. Bréchignac, Ph. Cahuzac, F. Carlier, M. de Frutos, J. Leygnier, J.Ph. Roux, J. Chem. Phys. **99**, 6348 (1993); C. Bréchignac, Ph. Cahuzac, M. de Frutos, P. Garnier, Z. Phys. D **42**, 303 (1997).
14. P. Labastie, J.M. L'Hermite, Ph. Poncharal, M. Sence, J. Chem. Phys. **103**, 6362 (1995).
15. R. Antoine, Ph. Dugourd, D. Rayane, E. Benichou, M. Broyer, J. Chem. Phys. **107**, 2664 (1997).
16. P. Lievens, P. Thoen, S. Bouckaert, W. Bouwen, E. Vandeweert, F. Vanhoutte, H. Weidele, R.E. Silverans, Z. Phys. D **42**, 231 (1997).
17. P. Lievens, P. Thoen, S. Bouckaert, W. Bouwen, F. Vanhoutte, H. Weidele, R.E. Silverans, Chem. Phys. Lett. **302**, 571 (1999).
18. P. Lievens, P. Thoen, S. Bouckaert, W. Bouwen, F. Vanhoutte, H. Weidele, R.E. Silverans, A. Navarro-Vázquez, P.v.R. Schleyer, J. Chem. Phys. **110**, 10316 (1999).
19. P. Lievens, P. Thoen, S. Bouckaert, W. Bouwen, F. Vanhoutte, H. Weidele, R.E. Silverans, A. Navarro-Vázquez, P.v.R. Schleyer, Eur. Phys. J. D **9**, 289 (1999).
20. W.A. de Heer, Rev. Mod. Phys. **65**, 611 (1993).
21. Ph. Dugourd, D. Rayane, P. Labastie, B. Vezin, J. Chevaleyre, M. Broyer, Chem. Phys. Lett. **197**, 433 (1992).
22. M.G. Burt, V. Heine, J. Phys. C **11**, 961 (1978).
23. C. Kittel, in *Quantum Theory of Solids* (John Wiley & Sons, New York, 1963).
24. M. Brack, Rev. Mod. Phys. **65**, 677 (1993).
25. M. Seidl, J.P. Perdew, Phys. Rev. B **50**, 5744 (1994).
26. F. Despa, Z. Phys. D **37**, 347 (1996).
27. G.D. Mahan, W.L. Schaich, Phys. Rev. B **10**, 2647 (1974).
28. R.M. Dreizler, E.K.U. Gross, *Density Functional Theory* (Springer, Berlin, 1990).
29. R.G. Parr, W. Yang, *Density Functional Theory of Atoms and Molecules* (Oxford University Press, New York, 1989).
30. R.O. Jones, in *Clusters of Atoms and Molecules (I)*, edited by H. Haberland (Springer, Berlin, 1995), p. 67.
31. J.P. Perdew, S. Kurth, A. Zupan, P. Blaha, Phys. Rev. Lett. **82**, 2544 (1999).
32. S. Kurth, J.P. Perdew, Phys. Rev. B **59**, 10461 (1999).
33. H.F. Budd, J. Vannimenus, Phys. Rev. Lett. **31**, 1218 (1973).
34. J. Callaway, *Quantum Theory of the Solid State* (Academic Press, New York, 1974).
35. R. Monnier, J.P. Perdew, D.C. Langreth, J.W. Wilkins, Phys. Rev. B **18**, 656 (1978).
36. J. Perdew, V. Sahni, Solid State Commun. **30**, 87 (1979).
37. C.Q. Ma, V. Sahni, Phys. Rev. B **19**, 1290 (1979).
38. Webelements, `http://www.shef.ac.uk/chemistry/web-elements/`
39. N.W. Ashcroft, N.D. Mermin, in *Solid State Physics* (Saunders College Publishing, Forth Worth, 1976).
40. N.D. Lang, W. Kohn, Phys. Rev. B **3**, 4555 (1971).